



Capacitor Voltage Control and Harmonic Suppression of Modular Multilevel Converter

Jingxuan Sun

School of Measurement and Control Technology and Communication Engineering, Harbin
University of Science and Technology, Harbin, 150080, China
sunjingxuan37@gmail.com

Abstract. The Modular Multilevel Converter (MMC) utilizes cascaded submodules to form a converter. As the number of submodules increases, higher output voltages can be achieved, making them suitable for medium and high voltage applications. They offer advantages such as low losses, high transmission efficiency, low switching losses, and reduced output harmonics. This paper investigates an MMC based on half-bridge submodules. Capacitor voltage control utilizes a combination of nearest-level approximation modulation and capacitor voltage balancing, employing a bubble sorting algorithm. This PI controller based on a feedback mechanism, the problem of circulating currents was solved by removing the coupling between the two feedback loops and obtaining two separate closed-loop control systems, the external control loop and the internal control loop. The results show that the circulating current is more stable, the distortion of the bridge current is reduced from 10.75% to 3.77%, the double-frequency content is greatly reduced. The simulation model was built with MATLAB-Simulink. The circulating current suppression effect is good, and the capacitor voltage waveform is stable. After the circulating current is suppressed, the rated current capacity of the power switching device can be reduced, which can reduce system costs and better extend the life of the power switching device.

Keywords: Modular Multilevel Converter, PI control, Nearest Level Modulation.

1 Introduction

In recent years, in order to achieve the "dual carbon" goal, new energy generation methods such as wind power are gradually being paid attention to [1-3]. Modular multi-level converters have been widely used in new energy fields such as wind power due to their advantages, such as higher voltage regulation range, lower harmonic content, and better fault tolerance. The concept of MMC was first proposed by German scholars in 2001 [4-5], and Siemens used it in actual projects in 2010. Since 2010, there have been more and more projects based on MMC. According to incomplete statistics, 30 projects have been put into operation. Foreign projects are concentrated in Europe, mainly for off-shore wind power transmission and grid interconnection; at the same time, the demand

for electricity and the quality requirements of electricity are gradually increasing, and the power transmission technology has also changed from DC transmission to DC hybrid transmission [6].

High Voltage Direct Current (HVDC) technology has the advantages of low line cost, large transmission capacity, high transmission efficiency and low transmission loss in the long-distance transmission of electric energy [7]. MMC forms a converter by cascading submodules. As the number of submodules increases, a higher output voltage can be achieved [8]. Therefore, HVDC based on MMC has many advantages in long-distance high voltage direct current transmission and has become the trend of future power transmission methods.

In contrast, the development of traditional two-level or three-level voltage source converter (VSC) has been restricted due to problems such as high harmonic content, low capacity, low voltage level, and dynamic voltage and current sharing when devices are connected in series. MMC-HVDC has been applied in many applications, such as rail transportation and solar power grid connection, and is particularly suitable for areas that require high voltage levels, large capacity, and high power [9-10].

This paper builds an MMC based on a half-bridge submodule. Capacitor voltage control utilizes a combination of capacitor voltage balancing and nearest-level approximation modulation. The proposed method ensures the stability of the convolution of the caps and effectively suppresses the second harmonic of the circulating current. The method of circulating current suppression consists of two closed loops, an outer voltage loop and an inner current loop, both controlled by a PI controller. Using MATLAB-Simulink, the success of this scheme is demonstrated.

2 MMC topology and mathematical model

2.1 MMC topology

Figure 1 shows the improved MMC topology structure, this method is applicable to the three-stage resonant power controllers with three symmetrical phases, each with a bridge circuit. The bridge circuit consists of N sub-modules and an inductor connected in a cascade structure to prevent circulating current between the three phases. Each submodule consists of a DC capacitor and a half-bridge unit. The MMC circuit topology is highly modular, allowing the number of connected submodules to be adjusted to meet various requirements. Perform a measurement within the box. When, V_{abc} is obtained U_{sq} and U_{sd} , L_{ac} enter the internal circuit. At this point, the model changes, and the entire output is treated as an ideal source.

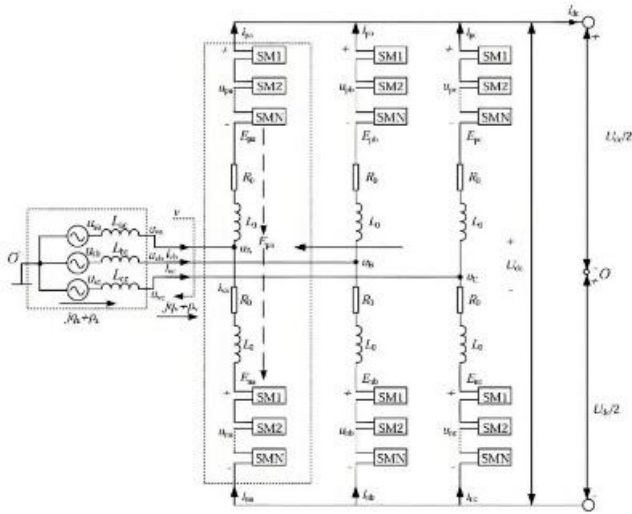


Fig. 1. MMC half-bridge topology.

2.2 Half-bridge submodule topology

Figure 2 shows the internal structure of the inverter. It is a half-bridge structure, and each half-bridge sub-unit is composed of two IGBTs and a group of capacitances.

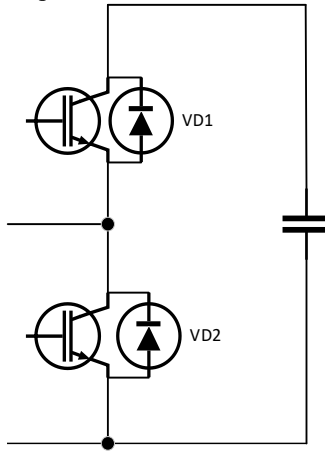


Fig. 2. MMC half-bridge topology.

By controlling the on/off state of the IGBT [11], the DC capacitor can be controlled to be in three working states: on, off, and locked. Affected by the current direction, each working state has two working modes. To avoid short circuit and cannot be turned on at the same time. Assume that the IGBT on state is recorded as 1 and the off state is recorded as 0. The working states of the half-bridge submodule are shown in Table 1.

Table 1. Font styles for a reference

		<i>i_{sm}</i> Direction is positive			<i>i_{sm}</i> and direction is negative	
T₁	1	0	0	1	0	0
T₂	0	1	0	0	1	0
U_{sm}	U_c	0	U_c	U_c	0	0
Working status	investment	resection	atresia	investment	atresia	resection

2.3 Mathematical model of MMC rectifier

The differential and common mode voltage equations based on KVL.

$$-\frac{U_{dc}}{2} + u_{pj} - R_0 i_{pj} - L_0 \frac{di_{pj}}{dt} - L_{sj} \frac{di_{vj}}{dt} + u_{sj} - u_{oo} = 0 \tag{1}$$

$$\frac{U_{dc}}{2} - u_{nj} + R_0 i_{nj} + L_0 \frac{di_{nj}}{dt} - L_{sj} \frac{di_{vj}}{dt} + u_{sj} - u_{oo} = 0 \tag{2}$$

U_{dc} is the direct current, u_{pj} is the upper voltage, u_{nj} is the lower voltage, i_{pj} is the upper current, i_{nj} is the lower current, u_{sj} is the side-grid voltage, i_{vj} is the side-grid current, and L_{sj} is the side-grid inductance.

Combining $i_{nj} - i_{pj} = i_{vj}$, $u_{diffj} = \frac{u_{nj} - u_{pj}}{2}$, (1) + (2) / 2 we get:

$$-u_{diffj} - \frac{R_0}{2} i_{vj} - (\frac{L_0}{2} + L_{sj}) \frac{di_{vj}}{dt} = u_{oo} - u_{sj} \tag{3}$$

Combining $u_{comj} = \frac{u_{nj} + u_{pj}}{2}$, $i_{cirj} = \frac{i_{nj} + i_{pj}}{2}$, (1)-(2)/2 we get

$$-\frac{U_{dc}}{2} + u_{comj} - R_0 i_{cirj} - L_0 \frac{di_{cirj}}{dt} = 0 \tag{4}$$

Let $R = \frac{R_0}{2}$, $L = \frac{L_0}{2} + L_{sj}$, through coordinate transformation and Laplace transform, the input and output model expressions of the MMC rectifier can be obtained as follows:

$$\begin{cases} (sL+R)i_{vd} = u_{sd} - u_{diffd} + \omega L i_{vq} \\ (sL+R)i_{vq} = u_{sq} - u_{diffq} - \omega L i_{vd} \end{cases} \tag{5}$$

Wherein, i_{vq} is the grid-side inductor current on the q-axis, i_{vd} is the grid-side inductor current u_{diffd} on the d-axis, is the differential-mode voltage on the d- u_{diffq} axis, is the common-mode voltage on the q-axis, u_{sd} is the grid-side power supply voltage on the d-axis, and u_{sq} is the grid-side power supply voltage on the q-axis.

The circulation model is:

$$\begin{cases} (sL_0 + R_0)i_{cir d} = u_{com d} - 2\omega L_0 i_{cir q} \\ (sL_0 + R_0)i_{cir q} = u_{com d} + 2\omega L_0 i_{cir d} \end{cases} \quad (6)$$

Wherein, $i_{cir d}$ is the current circulating on the d-axis, $i_{cir q}$ is the current circulating on the q-axis, and $u_{com d}$ is the common-mode voltage on the d-axis.

3 Simulation design and structure

3.1 Simulation parameters and structure e

The simulation submodule number $N = 18$, DC set voltage $U_{dc} = 25.2\text{kV}$, AC measured voltage $T_c = 6.6\text{kV}$, power level is 3.2MW , submodule voltage is 1400V , submodule capacitance is 1.5mF , voltage stabilizing capacitor is 1mF , and bridge arm inductance is 0.0577H .

The structures of the current inner loop and the circulating current suppressor are shown in Figures 3 and Figure 4.

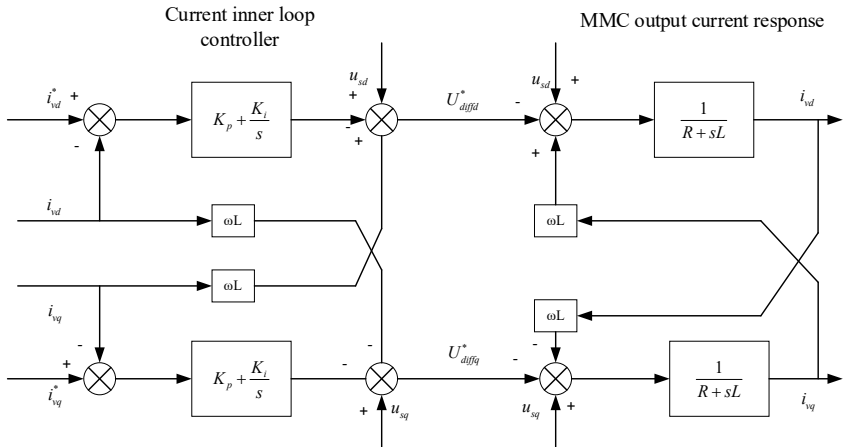


Fig. 3. MMC rectifier current inner loop.

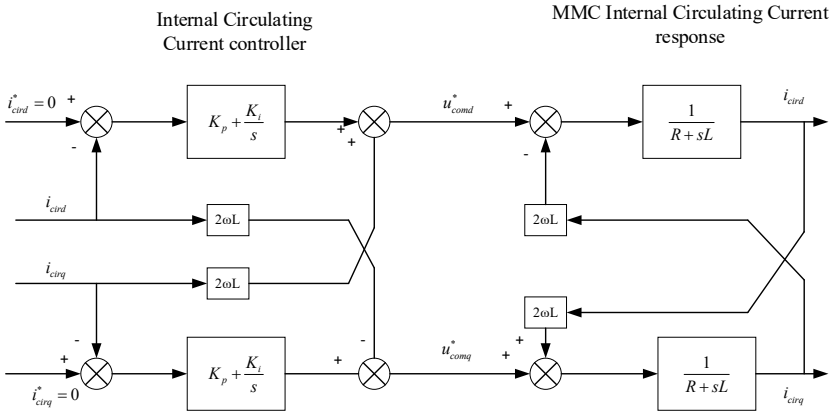


Fig. 4. Circulation suppressor.

The voltage outer loop is designed with DC voltage and adopts PI controller, as shown in Figure 5. The transfer function of PI control is:

$$G(s) = K_p + \frac{K_i}{s} \tag{7}$$

If s is a complex frequency domain variable, the integral time constant is denoted by K_i , and K_p is the proportional gain. Integral and proportional actions are combined in this transfer function. While the integral action removes steady-state errors, increasing system accuracy and stability, the proportional action reacts swiftly to system perturbations.

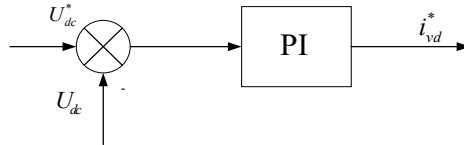


Fig. 5. Structure diagram of the MMC outer loop controller.

3.2 Nearest Level Modulation

Nearest Level approximation modulation is the most effective method for the PWM modulation of MMC, and the upper and lower bridge arms are able to produce $N+1$ -level stepped pulses, which, as N increases, become a sine wave with a higher fundamental, thereby reducing the harmonic content of the output voltage. The number of sub-modules required by the NLM modulation is calculated by using the instantaneous value of the triangle-wave modulating signal and the instantaneous value of the carrier wave, U_d , as follows:

$$\begin{cases} n_a = \frac{N}{2} - \text{round}\left(\frac{U_d}{U_c}\right) \\ n_b = \frac{N}{2} + \text{round}\left(\frac{U_d}{U_c}\right) \end{cases} \quad (8)$$

Among them, n_a and n_b are the number of upper and lower bridge arm input sub-modules respectively, in Figure 6.

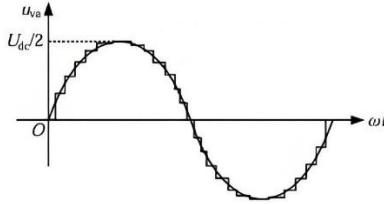


Fig. 6. Principle of nearest level approximation.

3.3 Control of capacitor voltage balancing

The voltage of the capacitors must be sorted in order to ensure the balance of the voltages. The charge and discharge of the two sets of capacitors are determined by the currents of the two arms of the bridge. Voltage division is based on sorting. Bubble sorting is used in the sorting process. Figure 7 illustrates the design sorting concept.

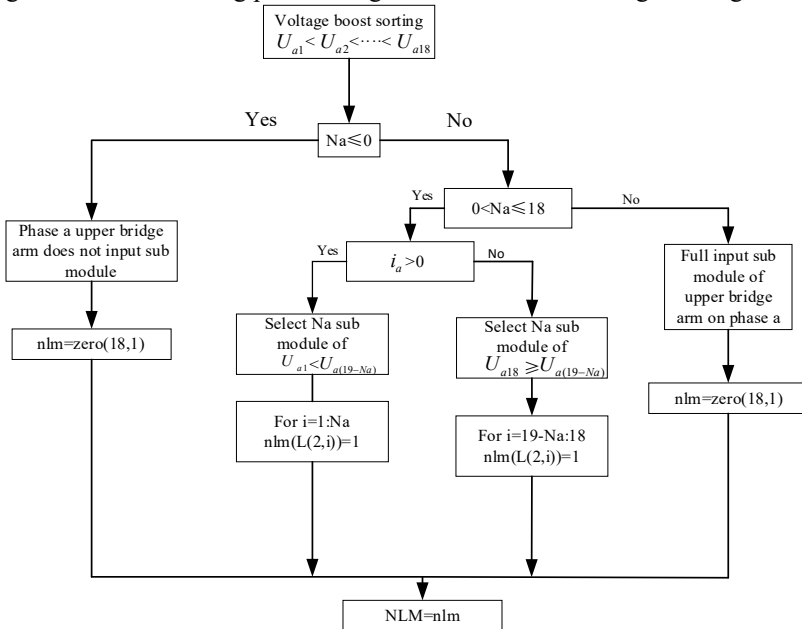


Fig. 7. Logic block diagram.

4 Simulation Verification

4.1 Circulation analysis

The simulation time is $t = 4s$, the control period is $T_c = 1e-4s$, and the circulating current suppressor is turned on at $t = 2s$. Figure 8 presents the waveforms both prior to and following the suppression of the circulating current.

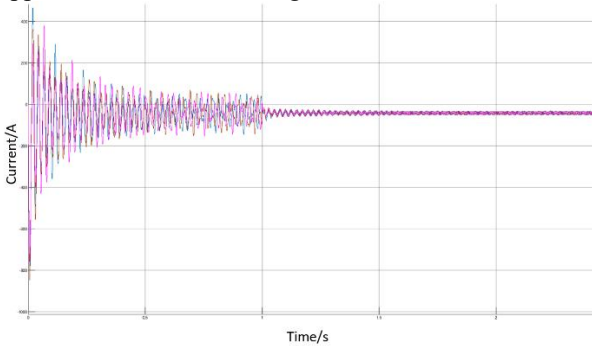


Fig. 8. Suppression circulation diagram.

Figure 8 makes it abundantly evident that the system's circulating current had a double-frequency component prior to circulating current suppression, which led to a high harmonic content. The circulating current is suppressed at $t = 2s$ when the PI controller is turned on and the circulating current suppressor is active. When this double-frequency component is reduced, the waveform of the circulating current gets closer to a steady value of $I_{dc}/3$. This illustrates how well the PI controller's circulating current suppressor works.

If we compare the waveforms of the current and distortion of the bridge before and after the elimination of the circulating currents, the effect of the elimination is clearly visible. The main source of circulating current, which greatly influences the current in the arm of the bridge, is the internal influence of the MMC. Figure 9 shows the bridge arm current diagram before reducing circulating current.

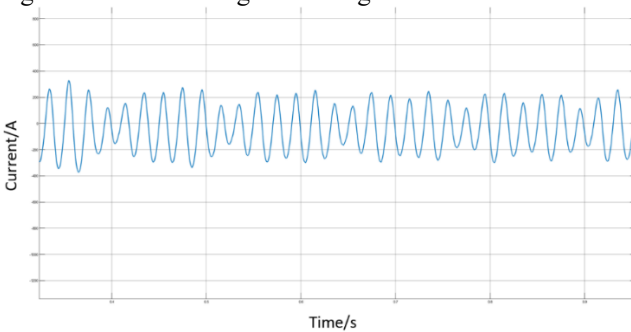


Fig. 9. Bridge arm current diagram before reducing circulating current.

Before circulating current suppression, the harmonic distortion of the arm current is high, and will have a bad effect on the arm equipment. The current THD of the bridge arm, using $t=0.5\text{s}$ and 15 cycles as an example, is 10.75%, as shown by FFT analysis. Figure 10 shows the bridge arm current THD.

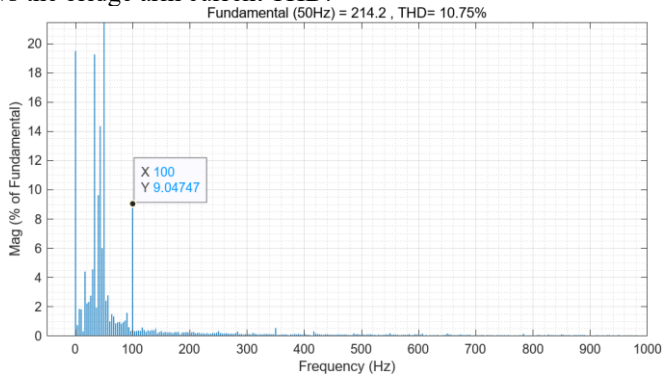


Fig. 10. THD diagram of bridge arm current before suppressing circulating current.

The double frequency content can be seen in Figure 10. It is evident that the circulating current has a substantial double frequency content—more than 9%. This suggests that the circulating current's harmonic components are substantial and need to be suppressed. The installation of the circulating current suppressor improves the bridge arm current. Figure 11 displays the bridge arm current waveform following suppression.

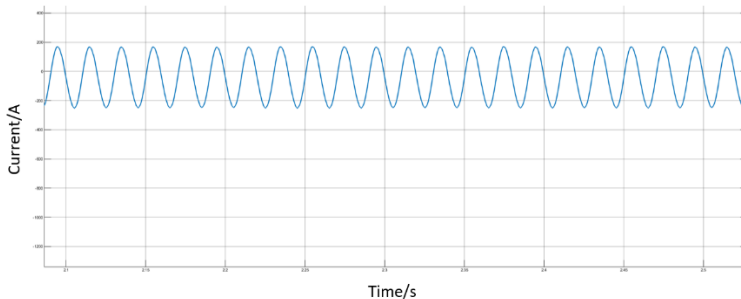


Fig. 11. Bridge arm current diagram after suppressing circulating current.

As seen in Figure 11, the bridge arm current waveform has been improved and the harmonic components have been significantly decreased. Using FFT analysis, Figure 12 displays the bridge arm current THD using $t = 3\text{s}$ and 15 cycles as an example. The position shown in the image represents the second harmonic content, and the bridge arm current THD is 3.77%. It is evident that the circulating current's second harmonic content, which was 3.6%, has been greatly reduced. The circulation suppression effect is nearly 65%, this confirms the effectiveness of the PI circulating current suppressor.

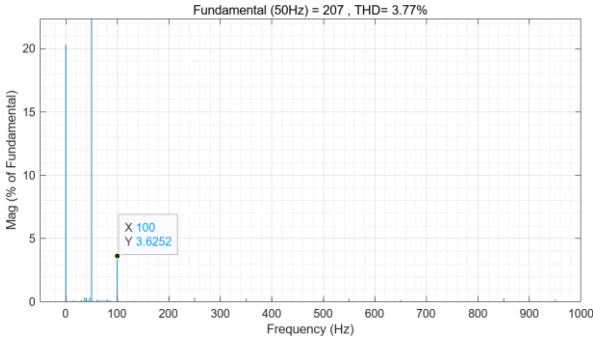


Fig. 12. THD diagram of bridge arm current after suppressing circulating current.

4.2 Capacitor voltage waveform

Through voltage balancing control, the capacitor voltage in each submodule can be seen. The capacitor voltage waveform is shown in Figure 13. The control period is 1e-4s. It can be seen that the capacitor voltage sorting effect in the simulation is good, the waveform is stable, and all submodules can be charged and discharged in an orderly manner according to the voltage balancing program, and the capacitor voltage fluctuation is small.

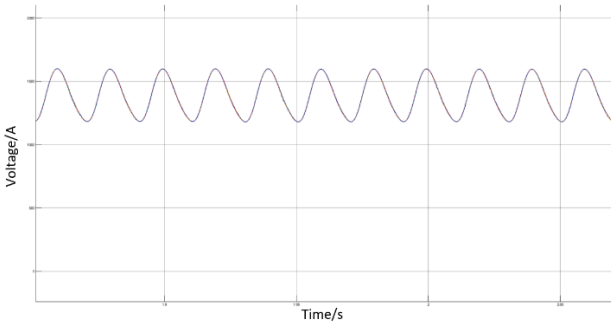


Fig. 13. Capacitor voltage waveform.

5 Discussion

The results of the present study show that the total harmonic distortion of the meter bridge current is reduced from 10.75% to 3.77% before and after the reduction of the circulating current. This reduction is due to the elimination of the second harmonic of the circulating current in the MMC. This reduces the current ripple in the bridge and protects the IGBTs in the bridge. The capacitor voltage shows a stable and narrow-banded waveform. Regarding circulating current suppression, the PI controller excels at DC reference tracking and disturbance rejection. However, a core limitation of the PI controller is that its inherent frequency response makes it difficult to provide suffi-

cient gain at twice the fundamental frequency, making it ineffective in suppressing circulating current disturbances at that specific frequency. Therefore, a resonant term is added to the PI controller at twice the fundamental frequency. This resonant term provides theoretically infinite gain at a specific frequency, enabling precise and error-free suppression of circulating current at that frequency, thus forming a proportional resonant controller.

6 Conclusion

This paper uses a multi-level converter based on a half-bridge sub-module as the basis, uses dual closed-loop control to solve the circulating current problem, adopts a PI controller as a circulating current suppressor, adopts capacitor voltage balancing control to solve the capacitor voltage balance problem, and adds a nearest level approximation modulation strategy for simulation analysis. Finally, the simulation proves that the capacitor voltage sorting effect of the model is good, the waveform is stable, and the circulating current is suppressed, which verifies the effectiveness of the proposed scheme. It can be better combined with high-voltage direct current transmission technology to improve transmission efficiency.

References

1. D. Zhang, C. Kang, X. Lu et al., Demonstration on the scale of energy storage deployment in high-proportion new energy power system. *Southern Power System Technology* 16, 3–11 (2022).
2. M. Stecca, L. R. Elizondo, T. B. Soeiro et al., A comprehensive review of the integration of battery energy storage systems into distribution networks. *IEEE Open Journal of the Industrial Electronics Society* 1, 46–65 (2020).
3. J. Li, X. Ni, P. Qiu, Review of flexible low-frequency AC transmission technology. *Zhongguo Dianji Gongcheng Xuebao/Proceedings of the Chinese Society of Electrical Engineering* 40, 42–50 (2021).
4. J. Rodriguez, J.-S. Lai, F. Z. Peng, Multilevel inverters: a survey of topologies, controls, and applications. *IEEE Transactions on Industrial Electronics* 49, 724–738 (2002).
5. A. Lesnicar, R. Marquardt, An innovative modular multilevel converter topology suitable for a wide power range, in 2003 IEEE Bologna Power Tech Conference Proceedings, (Bologna, Italy, June 23–26, (2003).
6. X. Zhao, C. Zhao, G. Li et al., Submodule capacitance voltage balancing of modular multi-level converter based on carrier phase shifted SPWM. *Power Capacitor* 31, 48–55 (2011).
7. F. Yu, H. Guo, L. Wang, Research on control strategy of multi-terminal photovoltaic MMC-MVDC system. *Electrical Measurement & Instrumentation* 43, 143–148 (2020).
8. M. Cao, Y. Wang, P. Liu et al., STATCOM model predictive control strategy based on modular multilevel converter. *Electric Drive* 52–56 (2013).
9. W. Wang, Z. He, G. Li et al., Recursive calculation method of MMC-HVDC DC fault current with AC effect. *Power Capacitor* 39, 313–320 (2019).
10. X. Guo, L. Liu, Y. Zhou et al., Overvoltage mitigation control strategies of MMC converter in a hybrid LCC-MMC HVDC system. *Global Energy Interconnection* 3, 412–419 (2020).

11. Q. Du, D. Li, J. Guo et al., Research on modular multilevel converter based on half-bridge submodule. *Energy Science* 62, 45–48 (2024).

Open Access This chapter is licensed under the terms of the Creative Commons Attribution-NonCommercial 4.0 International License (<http://creativecommons.org/licenses/by-nc/4.0/>), which permits any noncommercial use, sharing, adaptation, distribution and reproduction in any medium or format, as long as you give appropriate credit to the original author(s) and the source, provide a link to the Creative Commons license and indicate if changes were made.

The images or other third party material in this chapter are included in the chapter's Creative Commons license, unless indicated otherwise in a credit line to the material. If material is not included in the chapter's Creative Commons license and your intended use is not permitted by statutory regulation or exceeds the permitted use, you will need to obtain permission directly from the copyright holder.

